Interaction of Paraffin Wax Gels with Random Crystalline/Amorphous Hydrocarbon Copolymers

Henry S. Ashbaugh,[†,‡] Aurel Radulescu,[§] Robert K. Prud'homme,[†] Dietmar Schwahn,[§] Dieter Richter,[*,§] and Lewis J. Fetters[§,||]

Department of Chemical Engineering, Princeton University, Princeton, New Jersey 08544, and Institute for Solid State Research, Research Center, Jülich GmbH, D-52425 Jülich, Germany

Received March 18, 2002

ABSTRACT: The control mechanisms involved in the modification of wax crystal dimensions in crude oils and refined fuels are of joint scientific and practical interest. An understanding of these mechanisms allows strategies to be developed that lead to decreases in crude oil pour points or (for refined fuels) cold filter plugging points. The attainment of these goals involves the control and modification of wax crystals that spontaneously form in mixed hydrocarbon systems upon decreasing temperature. This work reports on the influence of random crystalline−amorphous block copolymers (ethylene−butene) upon the rheology of model oils. In a parallel fashion small-angle neutron scattering was exploited to gain microscopic insight as to how added poly(ethylene−butene) copolymers modify the wax crystal structures. The copolymers with different contents of polyethylene are highly selective with respect to wax crystal modification. Thus, the copolymer with the highest crystalline tendency is more efficient for the larger wax molecules while the less crystalline one is more efficient for the lower waxes.

Introduction

When paraffin waxes precipitate from oil, they form platelets of stacked lamella crystals that can fall into random "house of cards" structures (Figure 1) that readily entrain liquid oil, primarily through surface tension, effectively forming an organic gel.[1,2] This gelation is problematic in the recovery of crude oil from deep sea reservoirs, where there is a significant temperature and paraffin solubility drop between the reservoir and sea floor.[3−6] Moreover, the precipitation of large wax platelets from refined fuel stocks can clog engine filters and prevent operation under wintry conditions. Polymeric additives, which interact favorably with paraffins and moderate the wax crystal morphology, have been used to overcome these processing challenges. The mechanisms by which these polymers modify the wax structures, however, are incompletely understood. As such, the synthesis and choice of additives for crude oils and diesel fuels are largely trial and error rather than based on scientific principles.

Polymers with comb, diblock, and random architectures have found commercial application as wax modifiers. A trait that appears to be common among these additives is that the polymers themselves form self-assembled structures in oil. It is anticipated that the interplay between the polymer assembly and wax crystallization properties determines the efficacy of the polymer at moderating wax precipitation and gelation. Comb type polymers of poly(alkylacrylates), for example, cooperatively assemble in organic solvents into lamellar[7] and vesicular[8,9] structures having thicknesses comparable to that of the alkyl side chains depending on the degree of polymerization. Moreover, the degree of polymerization, and not necessarily the aggregate structure, dictates whether the polymer acts as a wax precipitation inhibitor (low molecular weight polymer) or promoter (higher molecular weight polymer) as a result of the relative solubility of the polymer in oil compared to that of wax.[10] When the wax precipitates at temperatures below the poly(alkylacrylate) assembly temperature, the supramolecular aggregate serves as a nucleation site for wax precipitation. From the standpoint of additive selection, it is interesting to note that comb polymers of fumarate vinyl acetate have been found to specifically target waxes of a given carbon chain length depending on the length of the polymer's alkyl side branches.[11]

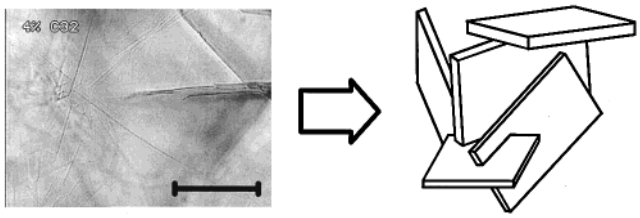

Figure 1. Optical micrograph depicting the morphology of 4 wt % C_{32} wax crystals in decane at 0 °C taken from ref 17. The solid bar corresponds to a length of 100 μm. The wax plates form a three-dimensional "house of cards" which traps oil in its interstitial spaces by surface tension effects forming a gel with a significant yield stress.

Diblock polymers of semicrystalline polyethylene coupled to amorphous poly(ethylene−propylene) (PE−PEP) or poly(ethylene−butene) (PE−PEB) spontaneously assemble in oil forming plateletlike supramolecular aggregates.[12,13] These platelets consist of a PE core shrouded behind an amorphous brush layer. The crystalline PE core serves as a nucleation site for wax precipitation, while the amorphous copolymer brush acts as a steric barrier keeping the aggregates in solution.[14−16] Rather than forming large plates themselves the wax is sequestered by the diblock micelles.

[†] Princeton University.
[‡] Present address: Los Alamos National Labs, Group T12, Mail Stop B268, Los Alamos, NM 87545. E-mail: hank@princeton.edu.
[§] Jülich GmbH.
[||] Present address: School of Chemical Engineering, Olin Hall, Cornell University, Ithaca, NY 14853.

10.1021/ma0204047 CCC: $22.00
Published on Web 07/25/2002

This mechanism for wax modification has found commercial application of PE−PEB (Paraflow) as diesel wax modifiers.

In applications[17] where the dissolved paraffin wax concentration is large, such as in crude oils, wax precipitation can bury the PEP or PEB brush layer, negating the steric stabilization benefit. Nevertheless, these crystalline/amorphous diblock copolymers are effective at breaking down wax gelled oil at very low concentrations.[17] This suggests that the polymer may interact with wax crystals in a capacity other than simply as a nucleator.

Random copolymers of ethylene and vinyl acetate (EVA-Paraflow) have found widespread use as pour point depressants for crude oil and petrochemical products. Viscometric[18] and light scattering[19] experiments have found evidence for intrachain as well as interchain associations between the microcrystalline ethylene units of EVA. More importantly, the efficacy of EVA as a pour point depressant is increased by increasing the extent of intrachain to interchain interactions.[20,21] This balance of associations is effected by the polymer molecular weight and degree of vinyl acetate content, as well as thermal history of the polymer solution.[18,22] The poorly characterized nature of these polymers (due to pronounced distributions in composition and molecular weight along with the potential for chain branching) and the miasma of variables affecting their interactions make correlation between the self-assembly properties of EVA and its wax modification capacity difficult at best. It is known that a fraction (∼50%) of the EVA nucleator material undergoes precipitation prior to any wax formation.[23] Thus, activity is diminished via the premature formation and precipitation of self-assembled aggregates.

Virtually random polymers of ethylene and butene (prepared by anionic polymerization of butadiene with variable 1,2- and 1,4-addition**)** are better suited for determination of their self-assembly and wax crystallization properties. Like EVA these polymers consist of microcrystalline ethylene units copolymerized with amorphous butene segments. The microcrystallinity of this polymer, designated PEB-*n*, where *n* is the number of ethyl side branches/100 backbone carbons, can be tuned by changing the ratio ethylene to butene segments, i.e., by varying *n* (for $n > 14$ crystallinity is absent in the bulk state). In this paper we examine the wax crystal modification properties of the PEB-*n* properties in the model system of paraffin wax (C_{24}−C_{36}) in decane. The ability of the polymers to moderate the flow properties of waxy oils is studied by characterizing the yield stresses of paraffin wax gels in decane doped with PEB-*n*. The microscopic interactions of the polymer with the paraffin waxes is studied using neutron scattering and the contrast variation technique to specifically identify the conformation and structure of the polymer and its effect on the wax precipitate. We find that the efficacy of the polymer at breaking down the wax gel structure correlates strongly with the self-assembly temperature of the PEB-*n* in solution. This is mirrored on microscopic scale where it is found that the polymer aggregates can serve as a template for wax precipitation or, depending on the solution conditions, the wax and polymer can cocrystallize in a synergistic supramolecular structure.

Experimental Section: Materials and Methods

Samples. Random copolymers of poly(ethylene−butene) of well-defined molecular weight and composition were prepared by anionic polymerization[24] followed by hydrogenation of the polydiene intermediate. The parent random polydiene samples were obtained by the polymerization of 1,3-butadiene in mixtures of hexane and triethylamine with *tert*-butyllithium as the initiator. The extent of 1,4-addition of butadiene (resulting in 2 ethylene units/butadiene unit) to 1,2-addition (yielding one butene unit) is tuned by varying the proportion of hexane (which favors 1,4-addition) to triethylamine (which enhances 1,2-addition) for a mixed polymerization solvent system. These polymers were subsequently saturated by hydrogenation at 80−100 °C under a pressure of 25−30 bar using palladium on barium sulfate as a catalyst, yielding the final random copolymers. These polymers are denoted PEB-*n*, where *n* is the number of ethyl side branches/100 backbone carbons. The parameter *n* was determined via H^1 NMR of the parent polydienes. We have examined (via rheology and SANS) PEB-*n*'s with *n* varying from 7.5 (semicrystalline) to 15 (amorphous) and molecular weights of $\sim 7 \times 10^3$ g mol^{-1}.

Model waxy oil samples for the rheology studies were prepared from paraffin waxes in *h*-decane (Sigma). Straight chain alkanes of carbon numbers (C_n) $n = 24$ (Sigma), 28 (Sigma), 32 (Aldrich), and 36 (Aldrich) were examined. The SANS data used *d*-decane while both per deuterated and hydrogenated versions of the linear alkanes mentioned above were used.

Paraffin Solubility. The solubility of *h*-C_n waxes in decane was determined in a Neslab temperature controlled bath accurate to within 0.1 °C. Samples ranging in wax concentration from 0.46 to 7.4 vol % (0.5 to 8 wt %) were prepared in sealed vials. The samples were initially heated above 70 °C to melt the wax crystals and then placed in the bath at 50 °C. At intervals of 30 min or more, the samples were visually inspected to determine if any precipitation had occurred and the temperature decreased in ∼1 °C increments. All the samples precipitate by 5 °C and, except for the lowest concentration C_{24} sample, did not flow upon ampule inversion at this temperature.

Yield Stress Measurement. The yielding behavior of waxy crude oils is complex and akin to the deformation and fracture of ductile solids.[25] Although compositionally homogeneous compared to crude oil, our decane solutions yield in a similar manner. In particular, once the gel network structure is broken by the application of stress, the wax particles settle and readily flow either with diminished or negligible yield stress. Here we are concerned with the initial breakdown of the gel.

Yield stress measurements were performed for sample mixtures of 4 wt % paraffin wax in decane as a function of PEB-*n* concentration over a range of temperatures up to the gel point. While the yield stress, τ_y, is defined as the stress below which no flow occurs, we adopt an operational definition of τ_y as the stress at the transition between the creep and liquidlike viscosity regimes. In this way, τ_y is identified as the stress for which the derivative is a maximum. These measurements are discussed in greater detail in ref 17.

The yield stress measurements were performed on a Rheometrics DSR controlled stress rheometer with a parallel plate geometry. The temperature was controlled to within 0.1 °C by a Peltier plate. The samples were initially heated to 70 °C to erase their thermal history and dissolve the PEB-*n* chains. To minimize evaporation, the sample was covered with a solvent trap and the temperature was rapidly decreased from 70 °C to the experimental test temperature. After the sample was allowed to anneal at constant temperature under no stress for 20 min, a static stress was applied and incrementally increased every 10 s (100 stress increments/decade) and the viscosity measured. Typically the initial applied stress was chosen well below the stress at which creep begins. While there is concern over the applicability of τ_y for crude oils to varying test geometries,[25] we are primarily concerned with the order of magnitude of τ_y and comparison of varying sample composi-

tions in the same geometry. The measured yield stresses were reproducible to within 10−20%.

Small-Angle Neutron Scattering: Theory. The aggregation of paraffin molecules in the presence of PEB-*n* random copolymers in dilute decane solution was investigated at the microscopic level by small-angle neutron scattering (SANS). The structures formed by the polymer and paraffin were studied separately by the contrast matching technique and analyzed in parallel with the case of the polymer self-aggregation in decane.

The small-angle scattering of neutrons arises from the fluctuations of the scattering length densities within a material $\rho_i = (\Sigma b_i)/v_I$, where b_i are the scattering lengths of the different atoms in a monomer or molecule i and v_i is the volume of the corresponding entity. For a multicomponent system containing polymer, paraffin, and solvent the scattering intensity may be described in terms of partial structure factors $P_{ij}(Q)$ according to

$$d\Sigma/d\Omega(Q) = (\rho_p - \rho_s)^2 P_{pp}(Q) + 2(\rho_p - \rho_s)(\rho_w - \rho_s)P_{pw}(Q) + (\rho_w - \rho_s)^2 P_{ww}(Q) \quad (1)$$

where "p" and "w" indicate the polymer and paraffin (wax), respectively, and "s" indicates the solvent used as a reference. The factor $\Delta\rho_{ij} = (\rho_i - \rho_j)$ represents the contrast between the components "*i*" and "*j*". As the scattering length density of the single components can be changed within given limits by hydrogenation or deuteration, samples can be prepared with either the polymer, $P_{pp}(Q)[\rho_w - \rho_s = 0]$, or the paraffin, $P_{ww}(Q)[\rho_p - \rho_S = 0]$, visible.

At high temperatures the polymer and paraffin molecules are dissolved in decane providing scattering from the single units. At low temperature large objects with a characteristic morphology are formed. The scattering from these objects can often be characterized by power laws according to

$$d\Sigma/d\Omega \approx Q^{-\alpha} \quad (2)$$

with the exponent α being characteristic for certain spatial arrangements.[26] In the case of a single polymer, one finds $\lambda = 1/\alpha$ (Flory exponent $\lambda = 3/5$ for swollen chains in a good solvent and $\lambda = 1/2$ for Gaussian chains at the Θ solvent condition). For aggregated structures one finds $\alpha = 1$ for rods and $\alpha = 2$ for platelets. Aggregates representing large 3-dimensional objects ($R > 1/Q$) with sharp interfaces give raise to Porod scattering with $\alpha = 4$. Exponents of $\alpha < 3$ and $3 < \alpha < 4$ can represent mass or surface fractal structures, while $\alpha > 4$ may be characteristic for diffuse interfaces.

Small-Angle Neutron Scattering: Experiment. The neutron small-angle diffraction experiments were performed at the SANS facilities installed at the FRJ-2 research reactor in Jülich in a Q range between $0.002 < Q < 0.14$ Å^{-1}. The data were corrected for scattering from empty cell and calibrated in absolute units by a Lupolen secondary standard.

First of all, the self-assembling behaviors of PEB-7.5 and PEB-11 random copolymers in decane were established by investigating the 1% polymer solutions over a large temperature range, between the single coil and the aggregates regime (85 to −30 °C). To achieve the maximum contrast and to minimize the incoherent background, fully protonated polymers were dissolved in fully deuterated decane (*d*-22).

Several mixed solutions of paraffins ($C_{24}H_{50}$ tetracosane or $C_{36}H_{74}$ hexatriacontane) and polymers (PEB-7.5 or PEB-11) in *d*-22 were then explored. The tetracosane and PEB-11 solutions were obtained by mixing different paraffin volume fractions (0.5, 1. and 2%) always with 1% polymer, while those of tetracosane and PEB-7.5 were prepared for 0.5, 1, 2, and 4% paraffin volume fractions and 0.6% polymer. The hexatriacontane and PEB-7.5 mixed solutions were studied for 0.5, 2, and 4% paraffin volume fractions and 0.6% polymer. The solutions were first heated to 85 °C to measure the single polymer and paraffin conformation. The samples were then gradually cooled to study the aggregation behavior. Aggregation could occur far below room temperature; the tetracosane and hexatriacontane solutions were investigated down to −30 and 0 °C, respectively. At a given temperature the SANS patterns of the polymer solutions remain unchanged during the measurements at different sample-to-detector positions and after different temperature cycles. So we are confident that the structures found represent at least very near equilibrium conditions.

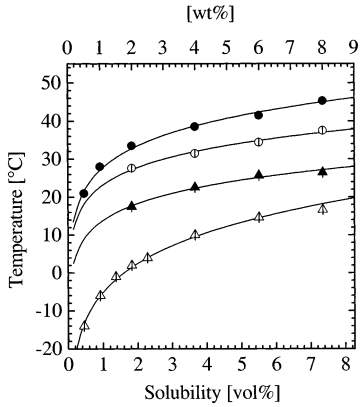

Figure 2. Observed cloud points of straight chain paraffin waxes in decane. The symbols denote the following: open triangles, C_{24}; closed triangles, C_{28}; open circles, C_{32}; closed circles, C_{36}. The lines correspond to the van't Hoff equation for the solubility fitted to the measured solubilities (eq 3).

Different contrast conditions (according to eq 1) were used to study separately the paraffin and the polymer conformation within the aggregates: (i) visible polymers, by using fully protonated polymers and matching the paraffin molecules with the solvent ($\rho_w = \rho_s$); (ii) visible paraffin molecules by using them in protonated state and matching the polymer with the solvent ($\rho_p = \rho_s$); (iii) for some systems only, both polymer and paraffin molecules visible, by matching them in hydrogenated state ($\rho_p = \rho_w$).

Results and Discussion

Paraffin Solubility and Gel Formation. The solubility in decane of the series of paraffin waxes considered here is shown in Figure 2. Not surprisingly, paraffin solubility decreases with increasing carbon number. If the log of the solubility, in mole fraction $x_{solubility}$, is plotted against the inverse of the absolute temperature, $1/T$, the dissolution enthalpy and entropy can be determined by fitting the solubility data to the van't Hoff equation

$$\ln x_{solubility} = -\Delta H_{dissolution}/RT + \Delta S_{dissolution}/R \quad (3)$$

where R is the ideal gas constant, assuming ideal solution behavior and a negligible heat capacity difference between the precipitate and dissolved wax. The chain length dependence of ΔH and ΔS was parametrized by a second-order polynomial. The solid lines in Figure 2 display the resulting fits.

Wax Gel Rheology. The yield stresses of the paraffin wax gels in decane without added polymer are shown in Figure 3. These yield stresses are on the order of 300 Pa and are essentially independent of temperature, except near the solubility boundary where the yield stress rapidly diminishes. This indicates that a sufficient amount of wax must precipitate from solution before a percolating gel network is formed. Indeed, because the C_{24} wax is the most soluble examined, the strength of this gel is most sensitive to temperature since C_{24} precipitates over the widest range of temperatures. The longer chain paraffins, on the other hand, precipitate over a relatively narrow temperature range,

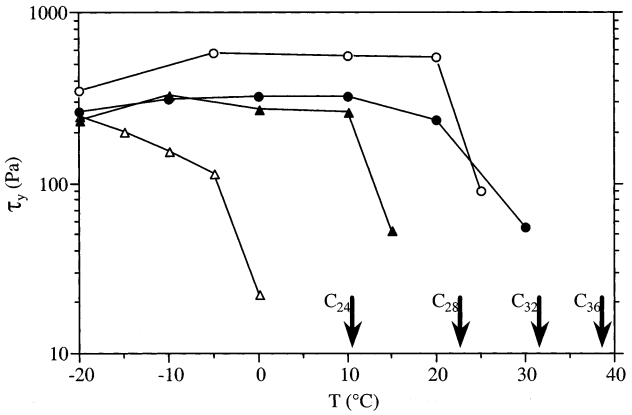

Figure 3. Measured yield stresses of 4 wt % straight chain paraffin waxes in decane as a function of temperature. The symbols correspond to the following: open triangles, C_{24}; closed triangles, C_{28}; open circles, C_{32}; closed circles, C_{36}. The arrows denote the cloud point temperatures of 4 wt % wax in decane reported in Figure 2.

more readily attaining a sample spanning structure with a yield stress. Notably, the C_{32} wax has a reproducibly higher yield stress than either the C_{28} or C_{36} waxes. While we do not have an definitive explanation for this observation, the key observation is that the plateau yield stress for all of these waxes lies within a range of 250−500 Pa at temperatures low enough to precipitate essentially all the wax from solution.

PEB-*n* significantly moderates the structure of the 4 wt % paraffin gels manifested macroscopically in the yield stress (Figure 4). In these figures we normalize the yield stress of the PEB-*n*-doped gels by the yield stress of the undoped gels at the same temperature:

$$\tau_{\text{relative}} = \frac{\tau_y(\text{with additive})}{\tau_y(\text{without})} \qquad (4)$$

These experiments were carried out at 0 °C, where the gels have essentially temperature independent yield stresses, except for the case of the C_{24} wax which were performed at −20 °C, where the yield stress of the undoped wax reaches that of the longer waxes. The polymer shows qualitatively similar effects on the yielding behavior of these paraffin gels as the PE−PEP diblock polymers examined in a previous study. In particular, PEB-*n* can reduce the gel yield stress by 3−4 orders of magnitude at polymer concentrations as little as 0.05 wt % or 500 ppm in decane. This is particularly significant for practical applications of this polymer as a wax crystal modifier since it is desirable to use as little of the additive as possible. With increasing PEB-*n* concentration the gel yield stress rebounds and increases up to levels comparable to the neat gel at polymer concentrations on the order of 1 wt %. We note in some cases at very low additions of the PEB-*n*, most apparent for PEB-15, polymer additions can increase the gel yield stress. However, this initial rise is only on the order of a factor of 2 and somewhat overshadowed by the reduction in the yield stress.

PEB-*n* demonstrates selectivity in paraffin wax modification depending on the microcrystallinity of its backbone. In the case of the longest C_{36} paraffin considered, it is found that PEB-7.5 is the most efficient reducing the gel yield stress (Figure 4a). That is it takes less PEB-7.5 to reach the minimum in the wax yield stress than any of the other PEB-*n*'s examined. The minimum

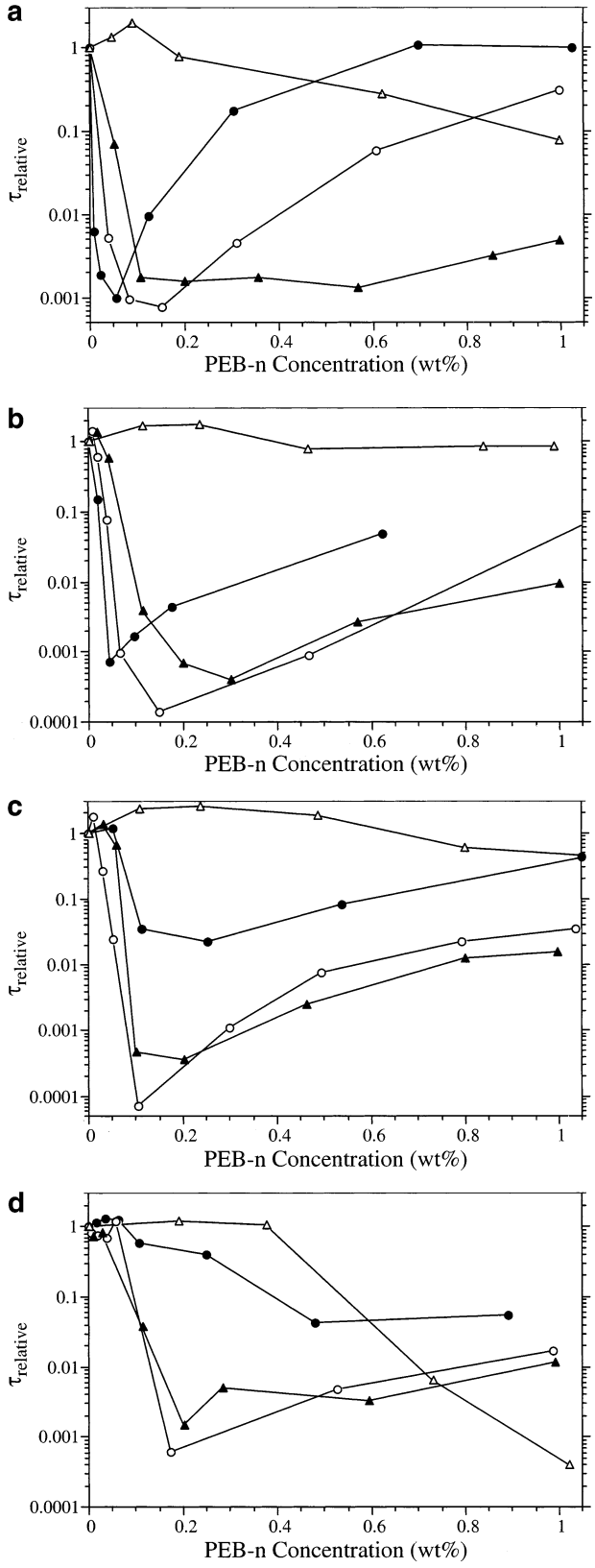

Figure 4. Effect of PEB-*n* concentration on the yielding behavior of 4 wt % wax gels in decane. The yield stresses are normalized with respect to the yield stress of the gel without any added polymer. The symbols denote the following: closed circles, PEB-7.5; open circles, PEB-10; closed triangles, PEB-11; open triangles, PEB-15. Results are reported for C_{36} wax (a), C_{32} wax (b), C_{28} wax (c), and C_{24} wax (d). All the experiments were conducted at 0 °C, except those for C_{24} wax which were conducted at −20 °C to ensure sufficient wax precipitation to form a gel.

in the gel yield stress is shifted out to increasing polymer concentrations with increasing number of ethyl side branches on the polymer backbone, i.e., decreasing polymer microcrystallinity. It is worth noting that the yield stress minimum appears to grow broader with increasing number of ethyl side branches, such that for PEB-11 the gel yield stress is minimal from nearly 0.1 wt % up to 1 wt % although slight increases in the yield stress are observed at the highest polymer concentrations. PEB-15, in comparison to the other polymers, has almost no effect on the gel yield stress, and a minimum yield stress is not observed below 1 wt % of the polymer in decane.

We may anticipate that the results for the C_{36} wax gels are related to the decreasing microcrystallinity with increasing of the PEB-*n* polymers with increased ethyl side branching. It is worthwhile to consider what would happen if we were to examine PEB-*n*'s with less than 7.5 ethyls/100 backbone carbons. In the extreme case of PEB-0, the polymer is essentially crystalline high-density polyethylene and is not soluble in oil except at very high temperatures that are well above the paraffin wax solubility boundary. At the temperatures where the wax falls out of solution and forms a gel, PEB-0 would have precipitated from solution at a much higher temperature and would be unavailable to effect the wax structure. It may be hypothesized that there exists an extent of side branching that the polymer most efficiently is incorporated into the wax crystals. Along this line of reasoning for the C_{36} wax discussed above, the most efficient polymer would have a degree of ethyl substitution of 7.5 or less. Rather than examine lesser degrees of ethyl side branching that would require synthesis of additional polymers, we consider the polymer effect on shorter, and hence more decane soluble, paraffin waxes.

In agreement with the C_{36} wax gels, the yield stress minimum polymer concentration monotonically increases from PEB-7.5 to PEB-15 for the C_{32} wax gels (Figure 4b). The preference for the polymers to the paraffin wax chain length becomes apparent for shorter paraffins. For the C_{28} wax gels the yield stress minimum for PEB-7.5 is shifted out to higher concentrations than that for both PEB-10 and PEB-11 (Figure 4c). This effect is exacerbated for the C_{24} waxes where not only is the yield stress minimum for PEB-7.5 shifted out to even greater polymer concentrations but in fact PEB-11 may be more efficient at breaking down the wax gel than PEB-10, though this is not a clear differentiation (Figure 4d). The present results strongly suggest, however, that the hypothesis presented above regarding the changing wax specificity of the polymers with changing ethyl content and microcrystallinity is correct. Moreover, these observations suggest that it may be possible to target and fractionate wax mixtures by tuning the polymer wax modifier microstructure.

When the yield stress of the PEB-7.5-modified wax gel is normalized by that of the unmodified gel at a given temperature, then the effect of the polymer additive is independent of temperature within the experimental accuracy; the minimum in the yield stress occurs at the same polymer concentration, and the magnitude of the yield stress reduction is the same.[17] It is particularly interesting to note that the yield stress of the unmodified C_{36} wax is fives times less at 30 °C than at 20 °C or lower temperature (Figure 3). That is, the extent of wax modification by PEB-7.5 is in direct proportion to the amount of wax precipitated and suggests that the PEB-7.5 is cocrystallizing with the C_{36} wax. A similar comparison with regard to the effect of temperature can be drawn for the interaction between PEB-11 and C_{36} wax, suggesting this conclusion is more general.

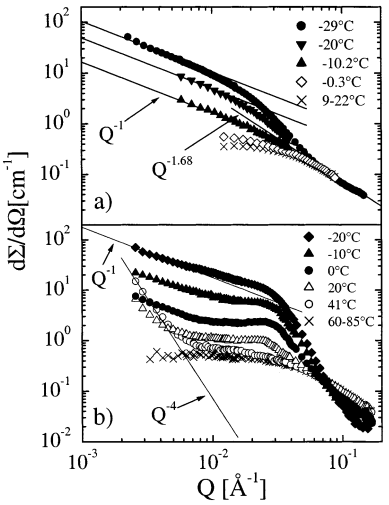

Figure 5. Small-angle scattering cross sections from solutions of PEB-11 (a) and PEB-7.5 (b) random copolymers in decane at a volume fraction of $\Phi_{pol} = 0.01$. The solid lines indicate the asymptotic power law scattering behavior at low Q according to eq 2.

Neutron Scattering. The self-assembly behavior of PEB-11 and PEB-7.5 in decane (*d*-22) can be deduced from the scattering profiles displayed in Figure 5a,b. Decreasing the temperature leads to a gradual increase of the scattering intensity at low Q for both polymer solutions indicating more pronounced aggregation of polymers at lower temperatures. For PEB-11, the copolymer with the higher density of ethyl side groups, the single chain regime extends over a broad range of temperatures, while, for PEB-7.5, the copolymer with the higher crystallization tendency, the single chain regime is found only for a limited range at high temperatures. Obviously, the aggregation process for each of the polymers in decane starts at different temperatures that are the lower, the higher the ethyl content is. While PEB-7.5 shows a tendency of slight but continuous aggregation already between 60 and 40 °C, PEB-11 starts to aggregate only below 0 °C.

The scattering cross section of both PEB-11 and PEB-7.5 polymers in the aggregation regime is characterized by a well-defined Q^{-1} power which is indicative for rodlike aggregates. The scattering profiles of PEB-7.5 exhibit in addition a correlation peak evolving at around $Q = 0.025$ Å^{-1} and, for the intermediate temperatures range (between 40 and 20 °C), a Q^{-4} behavior at low Q. The peak denotes a characteristic length of about 250 Å whose origin is not yet well understood. Possibly, it signifies some structure along the rod. The Porod scattering observed at higher temperatures is indicative for the formation of large aggregates featuring a well-defined surface. Its attenuation with decreasing temperature most likely results from coarsening processes which remove the scattered intensity of the initially formed aggregates out of the observation window of SANS.

The interaction of the PEB-*n* polymers with the paraffin either totally or partly changes the conformation and structure of polymer aggregates. This depends on the correlation between the polymer self-assembling

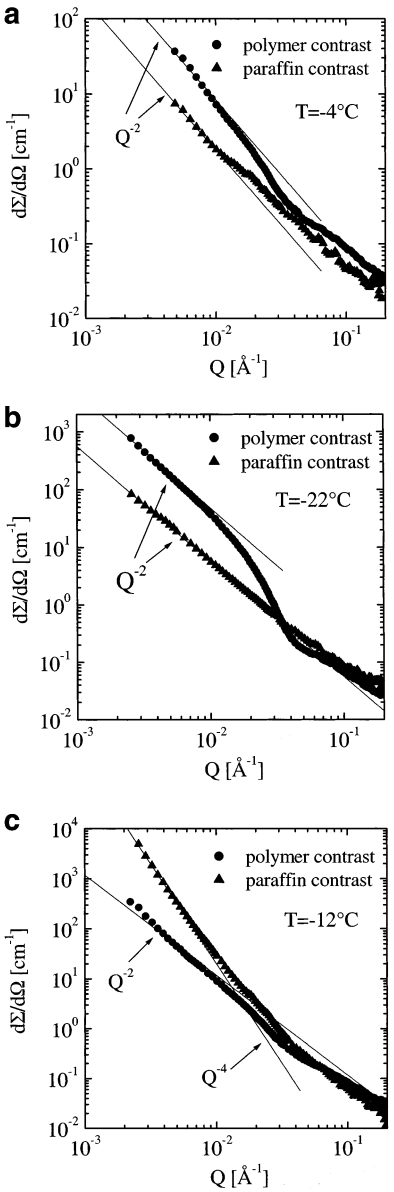

Figure 6. Small-angle scattering cross sections obtained at different temperatures from mixed solutions of PEB-11 ($\Phi_{pol} = 0.01$) and different volume fractions of $C_{24}H_{50}$ tetracosane in decane under polymer and paraffin contrast, respectively: (a) at −4 °C, for $\Phi_{wax} = 0.01$; (b) at −22 °C, for $\Phi_{wax} = 0.005$; (c) at −12 °C, for $\Phi_{wax} = 0.02$. The solid lines indicate the asymptotic power law scattering behavior at low Q according to eq 2.

temperature and the paraffin solubility point within the investigated range of the paraffin concentration. Some of the scattering profiles for the interaction of PEB-11 random copolymer with the tetracosane paraffin at different temperatures are presented in Figure 6 for small (a, b) and higher (c) amounts of paraffin added. At temperatures above 0 °C both polymer and paraffin are dissolved as single coils. At −4 °C (Figure 6a) both for polymer as well as for paraffin contrast at low Q the cross sections follow Q^{-2} power laws indicative for platelike structures. Thus, we find that the presence of the paraffin changes the aggregation behavior of PEB-11 from rodlike ($d\Sigma/d\Omega \sim Q^{-1}$) to platelike ($d\Sigma/d\Omega \sim Q^{-2}$) structures. As the temperature decreases (Figure 6b), (i) the intensity of both patterns strongly increases signifying the increased amount of aggregation and (ii) while the paraffin profile reveals a very extended Q^{-2} law indicating very thin plates, the polymer cross section decreases significantly below the asymptotic Q^{-2} law. This intensity modulation relates to the extended plate thickness of the polymer structure. For higher paraffin content (Figure 6c) 3-D paraffin crystals indicated by the Q^{-4} power law at low Q seem to coexist at low temperatures with the hairy plate structures that define the scattering at high Q. From a more detailed analysis presented in ref 27 a cocrystallization process of C_{24} and polymer into platelet structures is proposed where the very thin paraffin plates are monolayer tetracosane crystals with a thickness of 32 Å while the polymer structures are about five times as thick.

Figure 7 displays the scattering patterns of the mixed solutions of PEB-7.5 with different tetracosane contents for several temperatures of interest. In this case the polymer commences to aggregate earlier than the paraffin and develops its characteristic structures: the 3-D large aggregates at higher temperatures and the 1-D aggregates at lower temperature (Figure 5b). At 0 °C (still above the solubility line for 0.5% C_{24}) the intensity of the paraffin scattering profile shows a weak increase at low Q above the single coil form factor (Figure 7a). This behavior may be caused by small amounts of paraffin which associate with the preformed 1-D polymer structure. The tentative Q^{-1} power law defined by the scattered intensity at low Q and the narrow temperature range (slightly above the paraffin solubility line) support this idea. However, a slight deviation from the matching condition between polymer and solvent could produce a similar effect.

At temperatures below the paraffin solubility line, the scattering profiles observed under both contrasts change qualitatively and quantitatively and show that polymer and paraffin influence each others aggregation behavior (Figure 7b). On one hand, the paraffin aggregation influences the polymer structure which changes from rodlike (see Figure 5b; Q^{-1} power law) to a platelike (Q^{-2} power law) as in the case of PEB-11. Obviously cocrystallization of the polymer and paraffin takes place below certain temperatures. On the other hand, the paraffin scattering profiles reveal the correlation peak at the same position as for the polymer profiles (Figure 7b,c). We note that the peak position remains at the same Q as observed for the pure polymer solution (Figure 5b). Thus, the original polymer structure which is formed first influences significantly the common aggregation mechanism.

Though the mechanisms and the structural transformations which occur for this system by varying the temperature are not yet fully understood, from the experimental point of view we can offer some rationalizations. PEB-7.5 commences aggregation at temperatures above the wax solubility line thus permitting the formation of a primordial structure. This rodlike structure displays some density modulations along its axis, which may origin from correlated crystalline parts, followed by amorphous solvent swollen regions. When tetracosane starts to aggregate, the newly formed crystals associate first with the crystalline part of the self-assembled polymer structure and then, by continuous aggregation, extend into large 2-D objects involving more of the random copolymers by a cocrystallization process. The presence of a well-defined correlation peak in the scattering profiles of paraffin shows that the polymer apparently dictates to some extent the aggregation behavior of both materials. At low tempera-

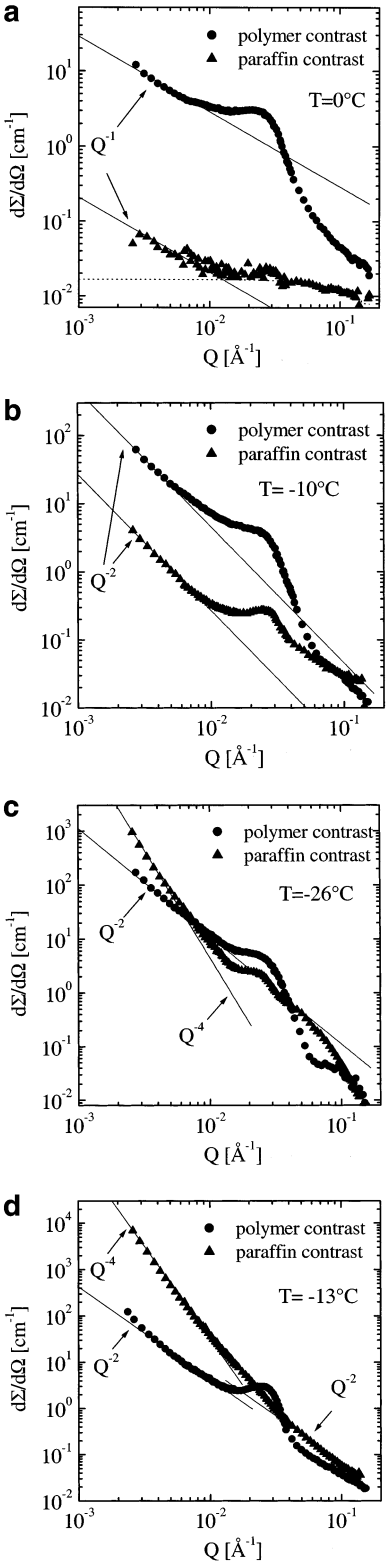

Figure 7. Small-angle scattering cross sections obtained at different temperatures from mixed solutions of PEB-7.5 ($\Phi_{pol} = 0.006$) and different volume fractions of $C_{24}H_{50}$ tetracosane in decane under polymer and paraffin contrast, respectively: (a) at 0 °C, for $\Phi_{wax} = 0.005$; (b) at −10 °C, for $\Phi_{wax} = 0.01$; (c) at −26 °C, for $\Phi_{wax} = 0.01$; (d) at −13 °C, for $\Phi_{wax} = 0.04$. The solid lines indicate the asymptotic power law scattering behavior at low Q according to eq 2.

tures (Figure 7c) or for the higher tetracosane content (Figure 7d), large 3-D objects appear to grow from the 2-structures (Q^{-4} behavior at low Q) while the copolymers remain anchored in the original plate structure.

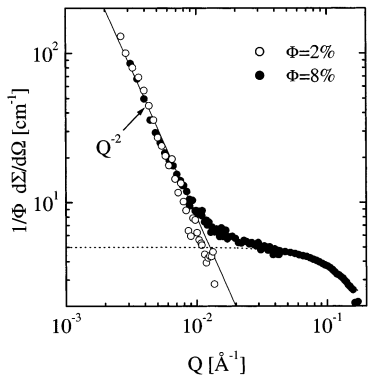

Figure 8. Small-angle scattering results from two solutions of $C_{36}H_{74}$ hexatriacontane in decane ($\Phi_{wax} = 0.08$ and 0.02) obtained at 80 °C. The asymptotic power law behavior at low Q is indicated by the solid line. The single coil form factor (Debye function) is shown by the dotted line.

A comparison of the SANS results obtained for the interaction of $C_{24}H_{50}$ tetracosane with PEB-11 and PEB-7.5 along with the wax rheology results is of interest (Figure 4a). We may conclude that the higher efficiency of PEB-11 compared to PEB-7.5 in breaking down the tetracosane gel is related to the closeness of the PEB-11 self-assembling properties and to the solubility line of tetracosane in decane. For that reason cocrystallization is fostered and the efficiency is high. PEB-7.5 aggregates initially independently and only partly together with the paraffin.

Before we discuss the interaction with $C_{36}H_{74}$ with the PEB-7.5 copolymer, we briefly report an unexpected result obtained from $C_{36}H_{74}$ solutions in decane at high temperatures. Figure 8 displays cross sections from 2% and 8% solutions at 80 °C well above the solubility line of this paraffin. The volume fraction normalized scattering profiles display a pronounced intensity increase at low Q. The data follow a Q^{-2} power law and show that even well above the solubility line the hexatriacontane paraffin forms plateletlike structures. It is interesting to note that the relative amount of the aggregate scattering appears to be independent of volume fraction. The volume fraction normalized profiles agree very well.

We may conclude that from a microstructural point of view this paraffin is not fully soluble in decane as molecules in solution appear to coexist with platelike structures.

The interaction of the hexatriacotane paraffin with the PEB-7.5 copolymer takes place in a fashion different from that of the tetracosane. Figure 9a−d presents scattering profiles for the polymer−paraffin interacting system captured at different temperatures and paraffin contents. The 2-D aggregates formed by the $C_{36}H_{74}$ molecules were observed at 77 °C even at the lowest paraffin content (Figure 9a). The corresponding polymer scattering profile also displays a Q^{-2} behavior indicating the formation of a similar structure by the polymer. This situation contrasts the pure PEB-7.5 self-assembling behavior in decane where the polymer stays in the single coil conformation at this temperature. Apparently, here the paraffin mediates the plate formation of the polymer.

Decreasing temperature leads to a joint aggregation process. The morphologies obtained are dictated by the paraffin tendency to form plates. Figure 9b displays Q^{-2} scattering profiles both for the polymer and for the

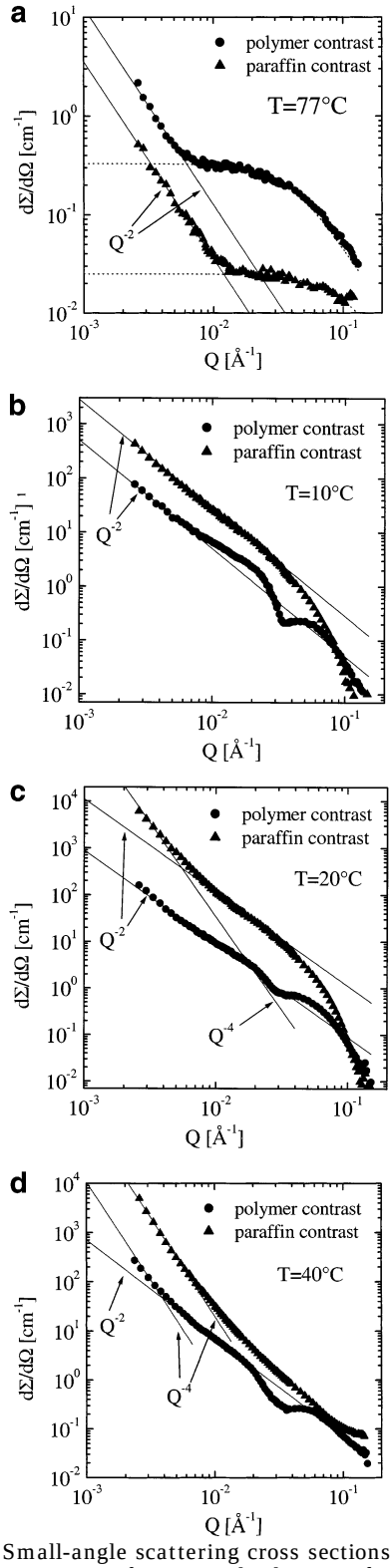

Figure 9. Small-angle scattering cross sections obtained at different temperatures from mixed solutions of PEB-7.5 (Φ_{pol} = 0.006) and different volume fractions of $C_{36}H_{74}$ hexatriacontane in decane under polymer and paraffin contrast, respectively. The following are a few examples which underline the qualitative results: (a) at 77 °C, for Φ_{wax} = 0.005; (b) at 10 °C, for Φ_{wax} = 0.005; (c) at 20 °C, for Φ_{wax} = 0.02; (d) at 40 °C, for Φ_{wax} = 0.04. The solid lines indicate the asymptotic power law scattering behavior at low Q according to eq 2.

paraffin. Within a narrow temperature range 3-D polymer objects coexist with these aggregates. The 2-D polymer−paraffin structures dominate over a wide range of temperatures and paraffin contents. For the

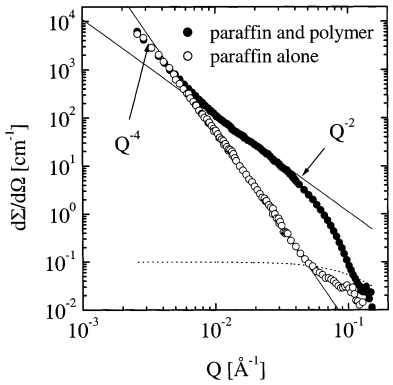

Figure 10. Small-angle scattering traces from two solutions of $C_{36}H_{74}$ hexatriacontane in decane (Φ_{wax} = 0.02) with and without PEB-7.5 random copolymer added (Φ_{pol} = 0.006) obtained under paraffin contrast at 20 °C. The power law behavior and the single coil form factor are indicated (solid and dotted lines, respectively).

paraffin case the Q^{-2} power law extends over a wide Q range and the deviations from the asymptotic Q^{-2} law at high Q yield information on the thickness of the paraffin plates (about 40 Å). For the polymer case the Q^{-2} dependence transforms at higher Q into an oscillatory behavior around the power law. A minimum at around Q = 0.035 Å^{-1} is followed by a peak structure that becomes evident around Q = 0.06 Å^{-1}. Such a profile is indicative of a polymer brush leaking out on both sides of the platelike core.[12]

For higher paraffin contents at low temperatures and low Q a strong upturn of the intensity is observed (Figure 9c,d). This tendency to Porod scattering is most strongly visible under paraffin contrast but is also observed by the profiles from polymer contrast. Obviously, large 3-D objects are formed. The scattering from these objects is particularly prominent for the highest paraffin concentration. We may conclude that a significant number of polymer−paraffin plates are created at intermediate temperatures (45−40 °C) and that the paraffin component grows quickly into the third dimension.

The wax crystal modification efficiency of PEB-7.5 may be observed directly from Figure 10, where we compare results from two 2% $C_{36}H_{74}$ solutions one with and the other without the polymer. Both experiments were done under paraffin contrast. The results are striking: the paraffin alone in decane forms large 3-D objects (well documented by the Q^{-4} power law). The addition of 0.6% copolymer causes the formation of the 2-D objects (Q^{-2} power law and a well-revealed platelet profile). Only over a limited Q range does the Porod law show the presence of additional 3-D aggregates. From these observations we may conclude that the interaction of the hexatriacontane paraffin with the PEB-7.5 random copolymer takes place by a cocrystallization mechanism, which is again a consequence of a good fit between the polymer and paraffin self-assembling properties. The rheological data for this paraffin show that PEB-7.5 is the most efficient copolymer regarding the breakup of the break the paraffin gel (Figure 4a). Obviously, the well-balanced wax−polymer cocrystallization process again does the job.

Finally, we wish to summarize the experimental findings in terms of "structural diagrams" for each of the investigated polymer−paraffin systems depicted in Figures 11−13. These structural diagrams display tem-

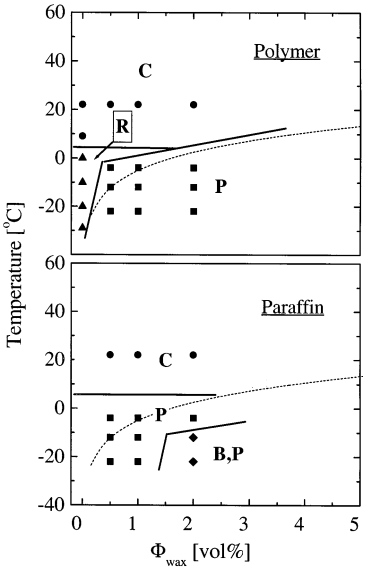

Figure 11. Temperature dependence of the polymer and paraffin aggregation behavior in mixed solutions of PEB-11 and $C_{24}H_{50}$ tetracosane as a function of the paraffin content (volume fraction Φ_{wax}) for $\Phi_{pol} = 0.01$. The capital letters denote the identified structures: C stands for coil conformation, R for rod structure, P for platelets, and B for 3-D bulk objects. The data points indicate the temperature volume fraction condition, where SANS experiments were performed. The symbols define a structural regime: filled circles, coils; filled squares, plates; filled triangles, rods; filled diamonds, plates and 3-D objects in coexistence.

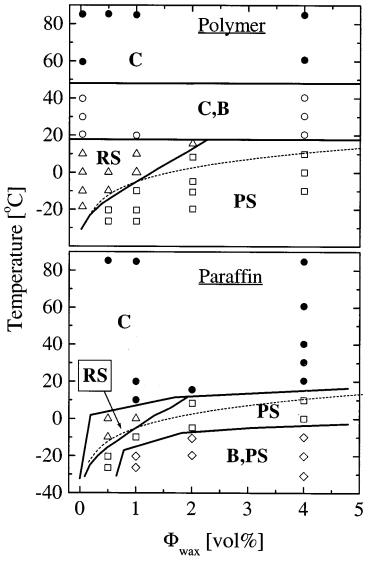

Figure 12. Temperature dependence of the polymer and paraffin aggregation behavior in mixed solutions of PEB-7.5 and $C_{24}H_{50}$ tetracosane as a function of the paraffin content for $\Phi_{pol} = 0.006$. Lines and symbols are as in Figure 11. In addition, there are the following symbols: RS, rods with possible density modulation along the axis (open triangles); PS, structurally correlated plates (open squares); open circles, 3-D objects and coil coexistence; open diamonds, structurally correlated plates and 3-D objects in coexistence.

perature versus wax volume fraction maps that indicate the different structures found by small-angle scattering experiments. Each symbol stands for one experiment, while the symbols itself indicate the structure found. In all cases, we distinguish between the polymer and the wax structures that are observed under the respective contrast conditions. We characterize the structural areas by the following symbols: C stands for coil conformation, R for rod or needlelike structures, P for plates, B for 3-D bulk structures, RS for rods with structural modulation along the rod, and PS for structurally correlated plates. The dashed line in each diagram signifies the wax solubility line; the solid lines separate regions of different structures.

Figure 11 displays the structural diagram for PEB-11 and $C_{24}H_{50}$ in decane. Under polymer contrast at temperatures higher than 0 °C polymer coil conformations are observed. Below this temperature and at low wax concentrations, rodlike precipitates start to appear. Below the wax solubility line, in all cases, polymer plates are found. For wax contrast the structural diagram is displayed for the same system. Above the solubility line, as expected, single wax molecules in coil conformation are found. Below and still slightly above the solubility line at small wax concentrations wax plate structures prevail while for a higher wax concentrations wax bulk phases start to appear seemingly crystallize from the polymer wax plates.

Figure 12 shows the polymer wax structural diagram for PEB-7.5 and $C_{24}H(D)_{50}$ in decane. Here the structure is more complex. Under polymer contrast we observe at temperatures above 45 °C single chain coil conformations. In the regime between 20 and 45 °C aside of the polymer coils, large 3-D objects are observed which appear to coarse grain with decreasing temperature. Below 20 °C, still above the wax solubility line and at low wax concentrations, we found rodlike structures with possible density modulations along the rod axis. At higher wax concentrations, still above the solubility line of the pure wax, polymer plate structures exhibiting interplate correlations appear. This structure covers the full low-temperature wax polymer regime.

Under wax contrast above 10 °C single wax molecules prevail. Below this temperature but already above the wax solubility line, there is some evidence for linear rodlike wax structures. In the regime, where the polymer displays correlated platelet structures at higher temperatures and lower wax concentrations, the same structure is observed also under wax contrast. For low temperatures and higher wax concentration wax bulk phases are present which appear to originate again from primary polymer wax cocrystallized platelets.

Finally, Figure 13 presents the results from the PEB-7.5 and $C_{36}H_{74}$ mixtures. Here we observe the most complex variety of structures. Under polymer contrast at high temperatures, a coexistence of polymer coil structures and polymer plates is seen. At zero wax concentrations below 45 °C (coil conformation structures excepted) 3-D bulk structures appear which vanish at around 20 °C. This is most likely again a consequence of coarse graining. At 10 °C and below, rodlike polymer structures appear which display internal structural modulations. The coexistence of single coil conformations and plates at low wax content and high temperatures is transformed at lower temperatures into an area (3 angular shape), where 3-D bulk structures and plates appear to coexist. At even lower temperature and higher wax concentration the bulk phases are not seen any more and plates are dominating the entire temperature wax concentration regime. At high wax concentrations three-dimensional polymer structures coincide with plates.

We now turn to the wax contrast. At high temperatures above 30−45 °C, depending on wax concentration,

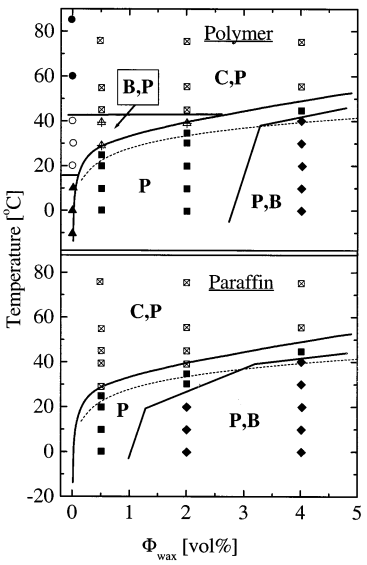

Figure 13. Temperature dependence of polymer and paraffin aggregation behavior in mixed solutions of PEB-7.5 and $C_{36}H_{74}$ hexatriacontane as a function of the paraffin content for $\Phi_{pol} = 0.006$. Lines and symbols are as in Figure 11 and 12. In addition, there are the following symbols: crossed squares, coils and plates in coexistence; crossed triangles, 3-D objects and plates in coexistence.

wax in solution and wax plate structures coincide. In a small temperature interval that narrows toward higher wax concentrations, plate structures dominate, while at lower temperatures plates and bulk structures coexist.

Conclusions

Solutions of semicrystalline random copolymers of ethylene and butene self-assemble into needlelike structures. However, in the presence of straight chain alkanes polymer/wax cocrystallization can occur with the formation of wax plates stabilized by the entrapped amorphous component of the copolymer. Yield stress measurements of the untreated model crude oils lie within the range of 250−500Pa at temperatures low enough for wax precipitation. However, treatment with the PEB-*n* at 500 ppm can cause 3−4 orders of magnitude decrease in yield stress of the gel network with the concomitant result that the wax particles settle and the system readily flows with either diminished or negligible yield stress. The PEB-*n* copolymers show selectivity in their paraffin wax modification capacities depending on the ethylene content of the backbones. The more crystalline copolymer (PEB-7.5) was the most efficient in reducing the gel yield stress of the longest paraffin considered, C_{36}. This suggests that efficient PEB-*n* additives for crude oils would contain graded ethylene contents.[28] Such crystalline−amorphous diblock or random copolymers can now be directly synthesized at ambient temperatures via the living polymerization of the respective olefins.[29] From the synthesis standpoint the crystalline segments can include s-polypropylene in addition to those that are ethylene based.

Acknowledgment. H.S.A. and R.K.P. gratefully acknowledge support from the Halliburton Co. We thank Drs. B. A. Pethica and M. Monkenbusch for ongoing constructive and enjoyable conversations with respect to this work.

References and Notes

(1) Abdallah, D. J.; Weiss, R. G. *Langmuir* **2000**, *16*, 352−355.
(2) Abdallah, D. J.; Sirchio, S. A.; Weiss, R. G. *Langmuir* **2000**, *16*, 7558−7561.
(3) Pedersen, W. B.; Hansen, A. B.; Larsen, E.; Nielsen, A. B.; Rønningsen, H. P. *Energy Fuels* **1991**, *5*, 908−913.
(4) Pedersen, K. S.; Skovbor, P.; Rønningsen, H. P. *Energy Fuels* **1991**, *5*, 924−932.
(5) Rønningsen, H. P.; Bjørndal, B.; Hansen, A. B.; W. B. P. *Energy Fuels* **1991**, *5*, 895−908.
(6) Hansen, A. B.; Larsen, E.; Pedersen, W. B.; Nielsen, A. B.; Rønningsen, H. P. *Enegy Fuels* **1991**, *14*, 419−430.
(7) Giorgio, S.; Kern, R. *Ultramicroscopy* **1987**, *21*, 157−170.
(8) Giorgio, S.; Kern, R. *Polymer* **1985**, *26*, 837−847.
(9) Ding, X.; Qi, G.; Yang, S. *Polymer* **1999**, *40*, 4139−4142.
(10) Kern, R.; Dassonville, R. *J. Cryst. Growth* **1992**, *116*, 191−203.
(11) Beiny, D. H. M.; Mullin, J. W.; Lewtas, K. *J. Cryst. Growth* **1990**, *102*, 801−806.
(12) Richter, D.; Schneiders, D.; Monkenbusch, M.; Willner, L.; Fetters, L. J.; Huang, J. S.; Lin, M.; Mortensen, K.; Farago, B. *Macromolecules* **1997**, *30*, 1053−1069.
(13) Lin, E. K.; Gast, A. P. *Macromolecules* **1996**, *29*, 4432−4441.
(14) Leube, W.; Monkenbusch, M.; Schneiders, D.; Richter, D.; Adamson, D.; Fetters, L.; Dounis, P.; Lovegrove, R. *Macromolecules* **2000**, *14*, 419−430.
(15) Monkenbusch, M.; Schneiders, D.; Richter, D.; Willner, L.; Leube, W.; Fetters, L. J.; Huang, J. S.; Lin, M. *Physica B* **2000**, *276−278*, 941−943.
(16) Buzza, D. M. A.; McLeish, T. C. B. *J. Phys. II* **1997**, *7*, 1379−1392.
(17) Ashbaugh, H. S.; Fetters, L. J.; Adamson, D. H.; Prud'homme, R. K. *J. Rheol.*, submitted for publication.
(18) Qian, J. W.; Qi, G. R.; Cheng, R. S. *Eur. Polym. J.* **1997**, *33*, 1263−1265.
(19) Qian, J. W.; Wang, X.; Qi, G. R.; Wu, C. *Macromolecules* **1997**, *30*, 327−331.
(20) Qian, J. W.; Li, J.; Zhou, G. H.; Qi, G. R. *J. App. Polym. Sci.* **2000**, *78*, 836−841.
(21) Qian, J. W.; Qi, G. R.; Han, D. L.; Yang, S. L. *Fuel* **1996**, *75*, 161−163.
(22) Qian, J. W.; Qi, G. R.; Fang, Z. B.; Cheng, R. S. *Eur. Polym. J.* **1998**, *34*, 445−447.
(23) Schwahn, D.; Richter, D.; Wright, P. M.; Symon, C.; Fetters, L. J.; Lin, M. *Macromolecules* **2002**, *35*, 861−870.
(24) Morton, M.; Fetters, L. J. *Rubber Chem. Technol.* **1975**, *48*, 359−409.
(25) Wardhaugh, L. T.; Boger, D. V. *J. Rheol.* **1991**, *35*, 1121−1156.
(26) Higgins, J. S.; Benoit, H. *Polymers and Neutron Scattering*; Clarenden Press: Oxford, U.K., 1994.
(27) Schwahn, D.; Richter, D.; Fetters, L. J.; Lin, M. *Macromolecules* **2002**, *35*, in press.
(28) Such copolymers could take the form of segmented materials, where *n* could cover the range of ca. 2−15 in going from segment to segment. It is also feasible that the change in *n* could be continuous.
(29) Tian, J.; Hustad, P. D.; Coates, G. W. *J. Am. Chem. Soc.* **2001**, *123*, 5134−5135.

MA0204047